PROCEEDINGS A

rspa.royalsocietypublishing.org

Research

Cite this article: Kudrolli A, Chopin J. 2018 Tension-dependent transverse buckles and wrinkles in twisted elastic sheets. *Proc. R. Soc. A* **474**: 20180062.
http://dx.doi.org/10.1098/rspa.2018.0062

Received: 31 January 2018
Accepted: 16 May 2018

Subject Areas:
mechanics, biophysics

Keywords:
thin sheet, twist, ribbon, elastic instability, buckling, wrinkling

Authors for correspondence
A. Kudrolli
e-mail: akudrolli@clarku.edu
J. Chopin
e-mail: julien.chopin@ufba.br

Tension-dependent transverse buckles and wrinkles in twisted elastic sheets

A. Kudrolli[1] and J. Chopin[2]

[1]Department of Physics, Clark University, Worcester, MA 01610, USA
[2]Instituto de Física, Universidade Federal da Bahia, Salvador-BA 40170-115, Brazil

JC, 0000-0001-5105-4437

We investigate with experiments the twist-induced transverse buckling instabilities of an elastic sheet of length L, width W and thickness t, that is clamped at two opposite ends while held under a tension T. Above a critical tension T_λ and critical twist angle η_{tr}, we find that the sheet buckles with a mode number $n \geq 1$ transverse to the axis of twist. Three distinct buckling regimes characterized as clamp-dominated, bendable and stiff are identified, by introducing a bendability length L_B and a clamp length $L_C (< L_B)$. In the stiff regime ($L > L_B$), we find that mode $n = 1$ develops above $\eta_{tr} \equiv \eta_S \sim (t/W)T^{-1/2}$, independent of L. In the bendable regime $L_C < L < L_B$, $n = 1$ as well as $n > 1$ occur above $\eta_{tr} \equiv \eta_B \sim \sqrt{t/L}T^{-1/4}$. Here, we find the wavelength $\lambda_B \sim \sqrt{Lt}T^{-1/4}$, when $n > 1$. These scalings agree with those derived from a covariant form of the Föppl-von Kármán equations, however, we find that the $n = 1$ mode also occurs over a surprisingly large range of L in the bendable regime. Finally, in the clamp-dominated regime ($L < L_c$), we find that η_{tr} is higher compared to η_B due to additional stiffening induced by the clamped boundary conditions.

1. Introduction

Twisting, along with stretching and bending, is a fundamental loading that can be applied to an elastic object. As the seminal work of Coulomb and Saint-Venant on the elastic equilibrium of prismatic bars [1,2], the response of slender structures under torsion has played a pivotal role in the development of the theory of elasticity [3,4]. More recently, a large number of studies have focused on complex equilibrium shapes arising

THE ROYAL SOCIETY PUBLISHING

upon twisting rods with circular or rectangular cross sections due to strong geometrical nonlinearities [5–9]. We focus here on elastic structures such as sheets and ribbons, where the thickness is much smaller than the width. In this limit, the classical Kirchhoff rod theory is ill-suited to model such strongly shape anisotropic structures and do not accurately predict their torsional stiffness and morphological response [10,11]. Because flexural modes are far less costly energetically than in-plane deformations, thin sheets can undergo buckling instability to accommodate compressive stress [12].

While constrained buckling instabilities of elastic rods and sheets in planar configurations have gathered significant attention [13–22], the rich set of buckling and wrinkling patterns observed in elastic sheets upon twist is only being appreciated more recently [23,24], triggering further theoretical and experimental studies [25–29]. Below a critical dimensionless tension T_λ applied along the longitudinal direction, it is well known that a twisted sheet in the form of a ribbon wrinkles due to the development of compression at the centre of the ribbon for sufficient twist [30,31]. Twisting above threshold, the wrinkling region is found to widen until reaching the edge of the ribbon consistent with predictions from a recent far-from-threshold theory for ultra-thin sheets [19,25]. Furthermore, the wrinkling pattern exhibits a symmetry breaking along with a continuous localization of the elastic energy leading to the formation of a triangularly faceted helicoid [26]. The resulting structure called e-helicoid is obtained experimentally under small finite tension as opposed to the developable faceted helicoid which is obtained theoretically for inextensible sheets [32]. However, above T_λ, the ribbon is observed to buckle or wrinkle only in the transverse direction depending on ribbon thickness and length [23,24,33]. While the Föppl-von Kármán (FvK) equations commonly used for thin sheets do not give rise to development of destabilizing compression in the transverse direction with twist, an additional term arising from finite rotation effects was identified and included in the instability mechanism [24]. This addition enabled us to capture the thickness dependence of the observed critical twist.

Subsequently, Chopin *et al.* [25] proposed a covariant extension of the Föppl-von Kármán (cFvK) equations which offers a rigorous theoretical framework to address equilibrium shape of ribbons which significantly depart from a planar base state. They derived the analytical expression of the transverse and longitudinal stresses, solving perturbatively the cFvK equations using a small slope and small tension limit, and suggested the existence of various transverse instabilities depending on the normalized length L/W and thickness t/W, the normalized tension T, and the applied boundary conditions. It is noteworthy that other nonlinear plate models have already been developed to deal with finite displacements, including Koiter's plate and shell models [34,35]; however, no analytical prediction nor scalings have been made available so far in the context of a stretched twisted ribbon. Given the increasing need to assess the range of validity of existing nonlinear plate models incorporating both stretching and bending contributions to the elastic energy [35,36], it would be interesting to derive predictions from other plate models which can be validated with experimental measurements. In this respect, the twisted and stretched ribbon configuration appears as an ideal benchmark for testing existing models and developing others to capture detailed features.

For a fixed tension $T_\lambda \ll T \ll 1$, Chopin, Demery and Davidovitch's model predicts two distinct instabilities of helicoid base state, which was analysed in depth. They further conjectured a third instability for short ribbons where the base state is dominated by the clamp boundary condition. Previously in [24], we showed that the shape of a twisted and stretched ribbon is a helicoid with zero mean curvature and constant negative Gaussian curvature except near the edges. In this region, the clamp boundary condition (a) is not compatible with the helicoid geometry, and (b) inhibits lateral displacement. Thus, significant shear and transverse stresses are induced on the sheet. Based on energy comparisons between clamped sheet and helicoid ribbon, Chopin *et al.* [25] also argued that the extent of the deviations from helicoid is given by a clamp length L_C which scales as:

$$L_C = \nu(W^2/t)T^{3/2}. \tag{1.1}$$

Thus, for $L > L_C$, a twisted sheet is expected to exhibit a helicoid base state. However, the precise distribution of stress inside the clamp-dominated zone is as yet not known.

At the other extreme, in the ribbon limit ($L/W \gg 1$), much more is known about the distribution of stress in the helicoid base state [24,25]. With respect to stability against buckling, two factors come into play. One is related to a tension-induced stiffness penalizing unstable modes with large amplitudes, and the other to a bending resistance which penalizes modes with large curvature. The tension-induced stiffness is analogous to that found in self-supported stretched sheets, and in thin films supported on elastic substrates [14]. It is noteworthy that in the case of self-supported sheets, the tension-induced stiffness is not a mechanical constant but rather originates from nonlinear geometrical effects that dominate for large deflections [14,15,19,25]. In particular, the tension-induced stiffness increases with the applied tension and decreases with sheet dimensions. Furthermore, tension-induced stiffness in twisted sheets is negligible compared to bending resistance when the tension is below a characteristic tension $T_C = (L^2t^2)/W^4$ [25].

Instead of tension, we find it more convenient here to introduce a new characteristic length scale, called the bendability length scale:

$$L_B = \left(\frac{W^2}{t}\right)\sqrt{T}. \tag{1.2}$$

Thus, when $L \gg L_B$, tension-induced stiffness can be neglected. The bendability length is closely related to the more general concept of bendability number which has proven to be useful to address wrinkling instability in uniaxially stretched sheets [19]. There, a high bendability number corresponds to a very thin sheet with negligible bending resistance compared to tension-induced stiffness.

Thus, the various possible regimes originally organized by Chopin *et al.* [25] in terms of tension T can be recast in terms of L, L_B and L_C as follows.

(a) For very long lengths ($L \gg L_B$) or infinite length limit, the sheet buckles in the fundamental mode with a wavelength $\lambda \sim W$ when twisted above a critical twist angle which is L-independent. The transverse compression is balanced by the bending resistance alone, and that tension-induced stiffness can be considered to be negligible.

(b) For intermediate lengths ($L_C \ll L \ll L_B$) or long but finite lengths, they calculated that the sheet buckles into higher modes (or wrinkles) with a wavelength which is smaller than W at a critical twist angle which decreases with tension and the length to thickness aspect ratio. For these lengths, the transverse compression has to overcome not only bending resistance but also a tension-induced stiffness as well.

(c) For short lengths ($L \ll L_C$) where length and width of the sheets are comparable, the clamps can be important because the clamped boundary condition induces stretching which causes considerable deviations of the stress from that for a helicoidal base state. However, no predictions were available of this effect on the critical angle and wavelength.

Thus, while now significant theoretical progress has been made in [25] on the instabilities observed with twist, experiments have been lagging meanwhile. Experimental measurements that provide a thorough test of the scaling approach and the regimes of their applicability, as opposed to direct numerical simulations of the thin plate equations, are sorely needed beyond what was reported in our previous experimental work [24]. While the numerical results may be accurate, they also typically make use of assumptions such as constant thickness for expediency. Experiments along with the scaling approach can also yield simple forms for the dependence on material parameters which can be readily applied to other systems. Thus, our goal in this study is to provide the prefactors in addition to testing the derived scaling laws against materials with a wide range of Young's modulus.

In this paper, we discuss the transverse buckling instability in thin elastic sheets by measuring the critical instability angle and characterizing the wavelength of the buckling mode with twist over a wide range of sheet length, width and thickness. We find that the observed instabilities are consistent with the overall behaviour proposed, with the critical twist angle dependent on the

aspect ratios and the tension. However, some differences were also found. From our experiments, we identify three distinct transverse instabilities corresponding to three regimes with increasing sheet length while holding width constant. Namely, a clamp-dominated regime, a bendable regime and a stiff regime.

The clamp-dominated regime is typically reached for short sheet $L \lesssim L_C$. We demonstrate that the sheet destabilizes into higher buckling modes at relatively higher twist and shorter wavelength. We argue that the clamped boundary conditions at the ends inhibits out-of-plane deflection leading to a delayed buckling instability. In the bendable regime reached for intermediate length $L_C \lesssim L \lesssim L_B$, fundamental and higher-order buckling modes are observed above a L-dependent critical twist angle which scales as $\eta_B \sim \sqrt{t/L}T^{-1/4}$. When higher-order buckling develops, we find the wavelength $\lambda_B \sim \sqrt{tL}T^{-1/4}$. These scalings are consistent with theoretical predictions derived in the bendable regime [25]. However, quite surprisingly, we find in the bendable regime that the sheet destabilizes into the fundamental buckling mode over a significant range of length to width aspect ratio. In this case, the wavelength trivially scales as $\lambda_{tr} \sim W$, a feature that was not predicted by the theory. Finally, the stiff regime is identified by going to extreme lengths. The sheet is found to destabilize into the fundamental mode above a critical twist that scales as $\eta_S \sim t/WT^{-1/2}$ in full agreement with predictions in the long length limit. Thus, we find that the crossover length L_B between the bendable regime and the stiff regime is captured by the transition from length-dependent to length-independent critical twist, but not by the wavelength transition from higher modes to the fundamental buckling mode. We find that the crossover length between the L-dependent to the L-independent critical twist is well captured by L_B but the transition from higher modes to fundamental modes as L is increased is significantly overestimated.

2. Experimental system

An image of the apparatus used to perform the experimental measurements is shown in figure 1*a*. As in our previous study [24], the ribbon is held under clamped boundary conditions at two opposite sides and twisted about its symmetry axis. The clamps were specially designed to ensure that a wide range of sheets with widths up to 0.1 m and thicknesses up to 5×10^{-3} m could be accommodated while being tightly held. These precautions ensure that the sheets did not slip over the wide range of stresses which develop as the sheet is twisted. While the clamp at the top end could be rotated about the central axis, the bottom clamp was held in place by linear low friction guides which allowed the distance between the clamps to vary in order to apply constant longitudinal tensions to the ribbon by hanging appropriate weights. This design also ensured that the clamps stayed perpendicular to the axis of rotation. The sheet is twisted by an angle θ about the x-axis while being pulled at the two clamped ends with a constant force F which is applied along the x-axis with the help of linear guides. The materials used and their properties are listed in table 1. Then, the non-dimensional tension $T = F/(EtW)$, where E is the Young's modulus, and the normalized twist angle $\eta = \theta(W/L)$. In the experiments discussed in the following, we apply a tension $T > T_\lambda$, corresponding to the tension below which compressive stresses develop in the longitudinal direction that can give rise to longitudinal wrinkles [24,30]. All the reported measurements were performed with the length of the sheet parallel with gravity to avoid any catenary-like effects in playing role in the measurements. Limited experiments performed with horizontal orientation did not uncover any systematic deviations due to gravity on the onset of instabilities at least for sheet lengths less than 2 m which were so tested.

Laser profilometry is used to obtain the shape of the ribbon. Using this technique which is described in more detail in a previous report [37], the sheet is illuminated with a 633 nm Helium–Neon laser and a cylindrical lens system in a plane which is orthogonal to the x-axis. The illumination pattern is then imaged from an angle using a digital camera after the light passes through an optical bandpass filter which allows only the light from the laser to pass through to isolate away spurious light. An example image with the bandpass filter removed is shown in figure 1*b*. If the sheet is planar, the illuminated pattern appears as a straight line. The height of the

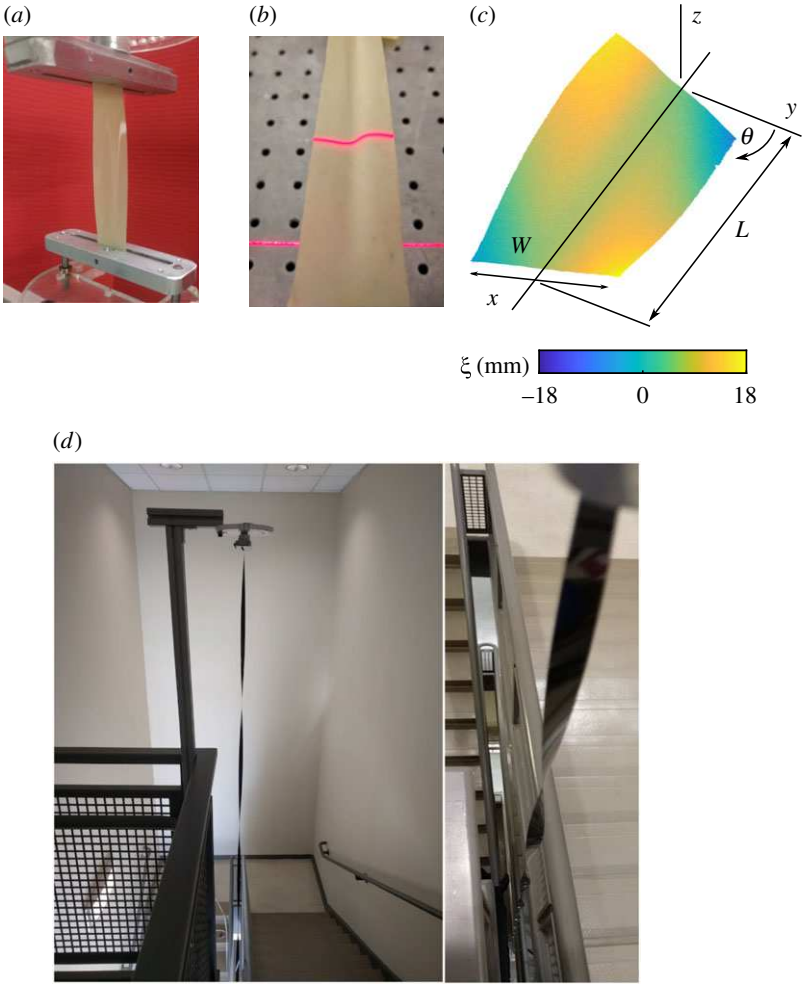

Figure 1. (*a*) An image of the apparatus and a wrinkled sheet which is clamped at its ends and twisted about its axis through an angle $\theta = 90^\circ$ (PolyVinyl sheet with $W = 50$ mm and $t = 152$ μm). (*b*) Angle view of a latex sheet illuminated by a red laser sheet ($W = 50$ mm and $t = 230$ μm). The intersection of a planar laser sheet with the wrinkled sheet is used to obtain the deflection of the ribbon surface. (*c*) A three-dimensional reconstruction of a wrinkled sheet obtained by sweeping the laser sheet ($\theta = 90^\circ$, $T = 0.1$, $L/W = 3$, $t/W = 0.0025$). The colour bar corresponds to the deflection $\xi(x, y)$ from the $x - y$ plane. (*d*) A side view image and a profile view of a twisted PET ribbon in the stairwell of the Math-Physics Building ($L = 16$ m, $W = 12.7$ mm). (Online version in colour.)

Table 1. List of various materials used in the experiments and their properties.

material	E (MPa)	ν	L (m)	W (mm)	t (μm)
polyvinyl	1.2	0.38	0.05–0.2	30, 50	230, 500
latex	3.2	0.50	0.08–2.0	50, 80	152, 500
PET	5700	0.37	0.10–16.0	3.8, 12.7	10, 18

sheet from a reference plane is then obtained by measuring the distance of the illuminated line from the point corresponding to the undeflected case. After sweeping the laser across the sheet surface, and calibrating for the viewing angle, we obtain the surface profile of the wrinkled sheet as shown in figure 1*c*.

The amplitude of the deflection $\xi(x, y)$ from the $x - y$ plane is also shown superimposed on the three-dimensional rendering of the sheet in figure 1*c*. One observes that the largest number of wrinkles and amplitudes occur at the midsection of the sheet, and decay smoothly to zero towards the clamped edges. This occurs because of the boundary conditions at $x = 0$, where $\xi = 0$ and $\partial\xi/\partial y = 0$ for $-W/2 \le y \le W/2$, and at $x = L$, where $\xi = y \tan\theta$ and $\partial\xi/\partial y = 0$ for $-W/2 \le y \le W/2$. Because we find the maximum deflection and the wrinkles occur along the central transect, we focus in the following on the profile observed in this cross section to identify the onset of the instability and the mode number. While the experiments were performed in the laboratory for lengths less than $L = 2$ m, about the height of the laboratory as shown in figure 1*a*, the stairwell in the physics department was used for longer lengths as shown in figure 1*d*. The clamps and the protocol used were otherwise the same.

3. Aspect ratio dependent instabilities

Figure 2 shows the mode number n as a function of sheet length to width aspect ratio L/W for a thin latex sheet ($t/W = 0.003$, $T = 0.08$). Example transects $\xi(x, y)$ at $x = L/2$ obtained using the laser profilometry above the onset of transverse instability are also shown for several L/W ratios. Because no moment is applied at the free edges, the transect appears to be curvature free at the edges. The mode number is then identified from the number of antinodes observed in the transect where the curvature passes through a maximum or minimum. Following the plot from right to left, one observes that n increases from $n = 1$ (fundamental buckling mode or buckle) to $n = 12$ (higher-order buckling mode or wrinkle) as L/W is decreased to 1 in this example.

Using equation (1.1) and equation (1.2) and substituting the material parameters corresponding to the elastic sheet used, we find that $L_C/W = 4$ and $L_B/W = 100$. Now, the theory [25] predicts that the ribbon wrinkles for $L < L_B$ with wavelength much less than the width W. Hence, it is worthwhile noting that the crossover between fundamental and higher-order buckling modes occur in the experiments for significantly smaller aspect ratio $L/W \approx 20$ according to our data than expected by the theory. However, it is unclear at the moment if the apparent discrepancy is due to a large numerical prefactor of order 10 in the scaling law, or due to a deeper issue with the derivation of equation (1.2). In particular, the range of validity of nonlinear plate models when stretching and bending contributions are of the same order of magnitude are still a matter of debate [21,35,36]. Hence, it will be interesting to see if other models can give a better account of the onset of higher-order buckling mode motivated by our observations.

(a) Length-dependent instabilities

We obtain the critical twist η_{tr} when a buckling mode starts to grow, by applying a prescribed tension and then slowly increasing the twist while monitoring the sheet deflection along the mid-transect of the sheet. Figure 3*a* shows the measured η_{tr} versus L/W plotted in log–log scale using the same experimental conditions as in figure 1*d*. We observe that η_{tr} decreases rapidly at first, before decreasing more steadily with L/W. We focus first on η_{tr} for relatively large length for which precise predictions are available. In the bendable regime ($L_C \ll L \ll L_B$), the helicoid base state becomes unstable against higher-order buckling modes above a critical twist that scales as [25]

$$\eta_B = \alpha_B \sqrt{\frac{t}{L}} T^{-1/4}, \tag{3.1}$$

for $\eta_{tr} \ll 1$ and $\lambda_{tr} \ll W$. Here, α_B is a numerical prefactor which is yet to be calculated, but can be determined from our data. The scaling is obtained from a linear stability analysis assuming a stretched helicoid base state. (Our previous experimental measurements of the ribbon morphology showed that this assumption is valid except very near the clamped edges [24].) This scaling corresponds to a line with slope 1/2 in the case where T and t are held constant, and is shown along with the data in figure 3*a*. We find that the observed η_{tr} is well aligned with

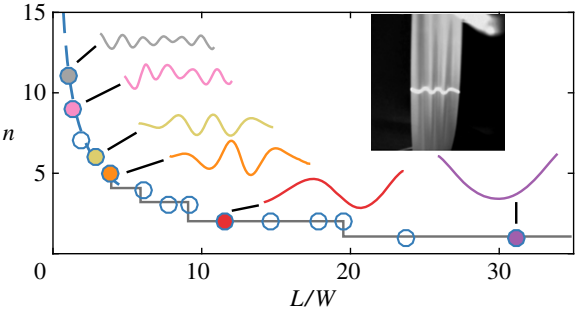

Figure 2. Observed number of modes decreases to one as the sheet length-to-width ratio is increased. Examples of observed transects at various L/W are also shown ($t/W = 3 \times 10^{-3}$). Inset: an example image used to extract the transects shown. (Latex sheet with $W = 50$ mm and $t = 152$ µm.) (Online version in colour.)

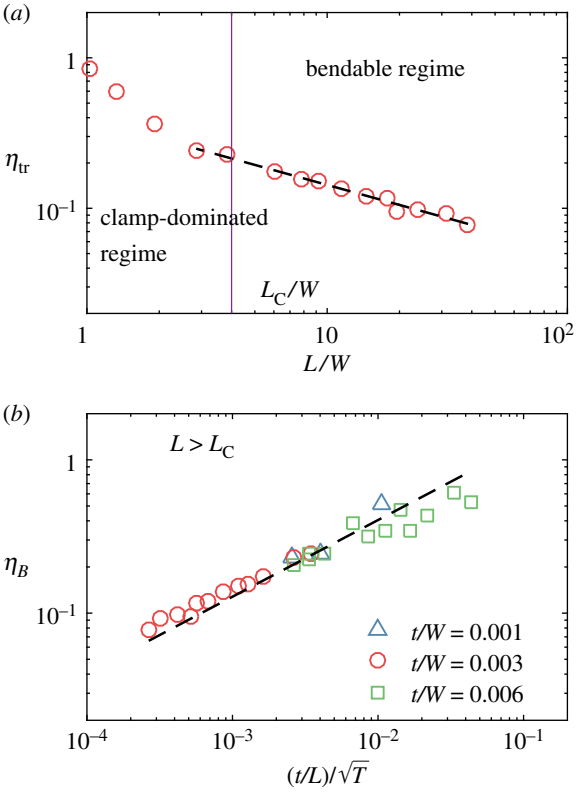

Figure 3. (*a*) Measured η_{tr} decreases as a function of L/W in log–log plot with slope consistent with 1/2 for $2 < L/W < 20$. The vertical line separates the clamp-dominated regime and the bendable regime. (*b*) The measured critical angle in the bendable regime η_B as a function of $(t/L)/\sqrt{T}$ corresponding to $L/W > 2$ collapses on to a line with slope 1/2. The data for $t/W = 0.001$ correspond to polyvinyl sheets, and for $t/W = 0.003$ and 0.006 correspond to latex sheets, respectively. The measurement error bars are smaller than the symbol size and thus not drawn for clarity. (Online version in colour.)

this prediction for $L/W > 2$. Interestingly, no change of scaling is observed at $L/W \approx 20$ when the instability reaches the fundamental mode $n = 1$.

We measure η_{tr} to test equation (3.1) in the bendable regime more extensively over a wide range of applied tension, sheet thickness, and materials listed in table 1. The observed η_{tr} in the

L-dependent regime where $L < L_B$, but above the point where edge effects start to dominate ($L > L_C$), is plotted in figure 3*b* as a function of $(t/L)/\sqrt{T}$. We observe excellent agreement with the predicted scaling and find $\alpha_B = 4.0 \pm 0.3$.

Now, the corresponding wavelength of the wrinkles in this bendable regime is given by Chopin *et al*. [25]

$$\lambda_B = \alpha_\lambda \sqrt{Lt} T^{-1/4}, \tag{3.2}$$

where α_λ is a numerical prefactor. Here, the scaling with tension can be noted to be the same as for longitudinal wrinkles [24]. The difference is the dependence here on sheet length L rather than the width W in the case of the longitudinal wrinkles [24].

The wavelength λ_{tr} obtained as $2W/n$ is plotted in figure 4*a* as a function of length and observed to increase like a staircase function till the maximum wavelength corresponding to twice the width of the sheet is reached. The data are observed to be well aligned with scaling given in equation (3.2) for $\lambda_{tr}/W \ll 1$, with systematic deviations growing as λ_{tr}/W approaches 1. This measured trend is consistent with the estimate calculated in [25] with systematically higher wavelengths for the thicker ribbon. Now, plotting λ_{tr} versus $(Lt)/\sqrt{T}$ for the latex as well as the PET sheets, we again observe good collapse of the data onto a line of slope 1/2 expected from the theory, provided $\lambda_{tr} < W$. We find that $\alpha_\lambda \approx 2.2 \pm 0.1$. It is noteworthy that the material parameters have been varied over three orders of magnitude in obtaining this data and gives a sense of the robustness of the scaling and the determined α_λ.

Thus, we find consistency with the prediction that wrinkling occurs in twisted sheets which depends on the applied tension in the limit of thin ribbons. This transverse instability occurs at lower twist angle with increasing tension. This is opposite even qualitatively to the trend at low tension where longitudinal wrinkling occurs [24,30]. In that case, the instability occurs at increasing twist angle as the tension is increased until the crossover tension T_λ is reached.

Furthermore, the points corresponding to the thicker latex ribbon ($t/W = 0.006$ and $L_B = 30$) can be noted to be especially interesting and may point to a larger range of validity for the scaling shown in equation (3.1) than implied by the calculation assuming $\lambda_{tr} < W$. In particular, it can be noted that for this thicker ribbon, η_{tr} is observed to scale consistent with equation (3.1) even though the fundamental mode is observed over a considerable part of this range. Thus, the scaling appears tied more strongly to the length dependence of η_{tr} rather than the condition that $\lambda_{tr} \ll W$. Further theoretical developments are still necessary to better understand this regime.

Focusing on the small L/W limit in figure 3*a*, where $L \sim L_C$, the trend in the data shows that elastic sheets become unstable and develop higher-order buckling modes above a critical threshold η_{tr} which is found to be significantly larger than the predictions given by equation (3.1). Further, the measured λ_{tr} is found to be slightly smaller than predicted by equation (3.2) in the same range of L/W. Here, we argue that edge effects are responsible for the significant deviations of the measured threshold and wavelength from predictions. We note that the prediction $L_C/W = 4$ is consistent with a change in scaling for η_{tr} (see dashed in figure 3*a*). This result suggests that the clamped edges are responsible for delaying the appearance of wrinkles for $L/W \gtrsim 1$, but do not suppress the instability.

The observed wrinkles in the clamp-dominated regime bear some similarity to tensional wrinkles observed at the centre of uniaxially stretched sheets [13,14,20,21,38]. However, it can be noted that transverse wrinkles under twist occur here for far greater ratios of t/W than observed under axial stretching alone [20,39]. Thus, the magnitude of compression which develops under twist is far greater than under uniaxial stretching alone due to the application of the tension. In that configuration, the uniaxial state of stress of a stretched membrane is frustrated by the clamped boundaries which induce shear and transverse stresses [40]. Therefore, development of transverse compressive stresses can give rise to an instability driven by the clamped edge stresses [14]. Later numerical studies indicate that the wrinkling instability, in fact, occupies only a bounded region of the L/W-T phase diagram [38]. However, in spite of these developments, the fundamental reason for the development of a compressive zone away from the boundary remains unclear.

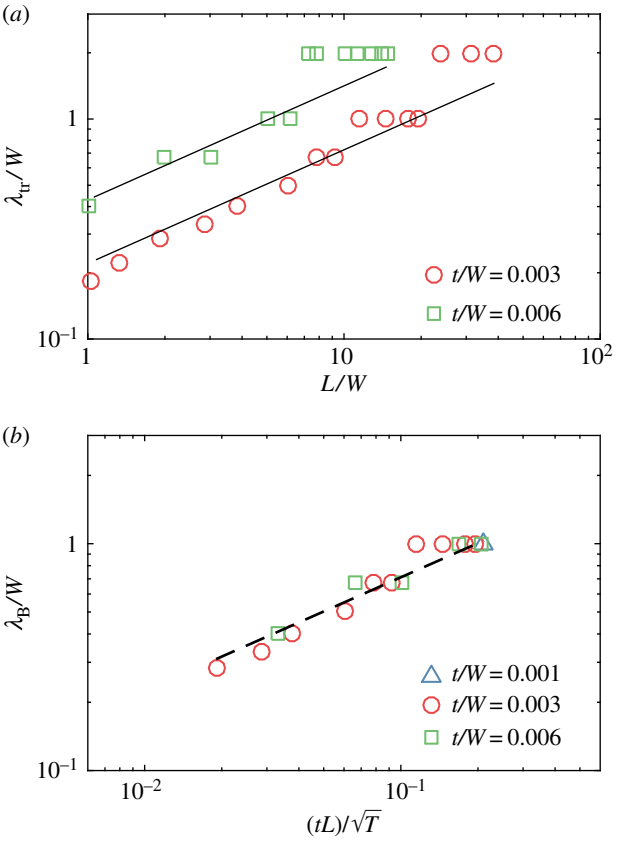

Figure 4. (*a*) The measured wavelength λ_{tr} as a function of L/W in log–log plot is observed to increase till the fundamental mode is reached where $\lambda_{tr} = 2W$. (*b*) The measured wavelength λ_{tr} as a function of $(tL)/\sqrt{T}$ collapses on to a line with slope 1/2 in the wrinkling regime when $\lambda < W$ consistent with predictions in the bendable regime. The data for $t/W = 0.001$ correspond to polyvinyl sheets, and for $t/W = 0.003$ and 0.006 correspond to latex sheets, respectively. The measurement error bars are smaller than the symbol size and thus not drawn for clarity. (Online version in colour.)

Now considering our twisted sheet configuration, we also argue that the frustration of the helicoid base state by the clamped edges is an essential ingredient to explain the delayed wrinkling instability. However, instead of giving rise to the wrinkling mechanism in axially stretched sheets, the clamped edges of a twisted sheet appear to act as a stabilizing effect in determining η_{tr}. We reach this conclusion because of the relatively higher rise in η_{tr} in the clamp-dominated regime compared to the bendable regime seen in figure 3*a*, and relatively lower wavelengths as well in figure 4*a*. A theoretical approach of the wrinkling mechanism in this regime which includes both twist and stretch loading at small L/W is not available, and is outside the scope of this study.

(b) Length-independent instability

In the limit where η_{tr} becomes independent of L, Chopin *et al.* [25] calculated that a novel buckling regime would be reached where the sheet destabilizes in the fundamental $n = 1$ mode at a critical twist angle in the stiff regime

$$\eta_S = \alpha_S \left(\frac{t}{W}\right) T^{-1/2}, \tag{3.3}$$

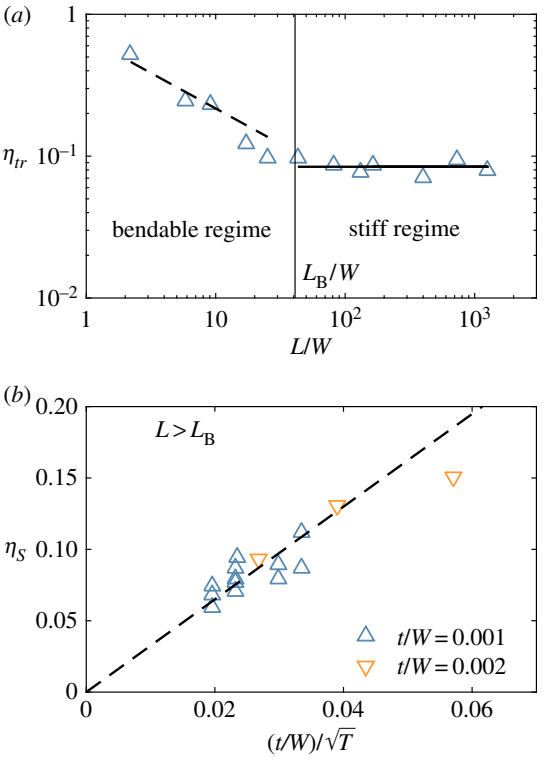

Figure 5. (*a*) η_{tr} crosses over from decreasing inversely as the length to becoming L-independent as the length is increased for the PET ribbon held at constant tension $T = 0.003$. The data are plotted in log–log scale. The crossover occurs as the contribution of the L-dependent tensional stiffening to the stability decreases to zero relative to the L-independent bending contribution. (*b*) The critical twist angle in the stiff regime η_S plotted as a function of $(t/W)/\sqrt{T}$ along with linear fit given by equation (3.3). The measurement error bars are smaller than the symbol size and thus not drawn for clarity. (Online version in colour.)

where $\alpha_S = 4.4$ was obtained numerically at large T. For small $T(< T_\lambda)$ and in the limit $\eta^2/T \gg 1$, the development of the longitudinal wrinkling instability far-from-threshold allows one to approximate the ribbon base state as being essentially a helicoid stretched in the vicinity of the free edges with a vanishing compression everywhere else. Using a linear stability analysis with reference to this post-buckling base state, $\alpha_S = \pi/\sqrt{3}$ was calculated analytically.

To reach this regime, we now consider extremely long ribbon experiments performed in the stairwell (figure 1*c*), in addition to those performed in the laboratory. The measured η_{tr} as a function of L/W for $L > 2$ m is shown in figure 5*a*. For $L < L_B$, we observe scaling consistent with equation (3.1), but then as L is increased above L_B, clear deviations are observed as η_{tr} occurs at a constant value within the error of measurements which is approximately $\pm 5\%$ in this case.

To understand the effect of this length independence on the scalings, $\eta_{\mathrm{tr}} \equiv \eta_S$ is plotted in a linear–linear scale as a function of $(t/W)/\sqrt{T}$ in figure 5*b* for the data corresponding to the L-independent regime. A linear fit according to equation (3.3) with $\alpha_T = 3.2 \pm 0.2$ is also shown which is consistent with previous calculations. However, significant deviations can be also noted from this form, which are somewhat higher than the error in the identification of η_{tr}. In the case of the PET ribbons used here, lowering the T resulted in approaching T_λ, the transition to the longitudinal limit, while increasing T beyond the reported range resulted in plastic deformation. Further experiments are needed to fully test this scaling over a wider range of T. However, this is beyond the scope of the materials available to us. Nonetheless, it is clear from figure 5*a* that the instability occurs at a much higher twist than predicted by equation (3.1), clearly demonstrating that the nature of the instabilities in the bendable and stiff regime is different.

To understand the two different mechanisms operating in the L-dependent bendable regime, and the L-independent stiff regime, we start by identifying the forces acting normal to the sheet and examining their relative contributions. Besides the transverse compressive force which is driving the instability, two stabilizing forces act on the sheet: a bending resistance penalizing large curvature, (or equivalently, small wavelength), and a tension-induced restoring force which prevents the development of large amplitudes. For large L/W, the tension-induced force is not sufficiently high to penalize the fundamental mode in favour of higher-order modes of smaller amplitude but larger curvature, thus the fundamental buckling mode is observed. As L/W is decreased, the tension-induced force is of the same order as the bending resistance, which indicates that wrinkling modes start to be energetically favourable. This crossover length between a L-dependent to a L-independent critical twist is observed to coincide well with the predicted L_B. By contrast, the transition from mode number $n = 1$ to $n > 1$ is observed to occur at a significantly smaller length than L_B.

4. Conclusion

We have experimentally studied the transverse wrinkling of a thin elastic sheet held under tension and twisted about its long axis. The critical twist is found to be not only dependent on the aspect ratio of the sheet but also on the applied tension along the axis around which the sheet is twisted. Three distinct regimes are identified, consistent with recent theoretical model of transverse buckling developed starting from a covariant form of the FvK equations.

To rationalize the different instability regimes, we introduced two characteristic lengthscales: a clamp length L_C and a bendability length L_B. When $L > L_B$, the instability is L-independent. We find that the sheet destabilizes in the fundamental buckling mode and that the critical twist decreases proportional to the thickness, and as inverse of the width and the square root of the applied tension. This instability occurs in the stiff regime as the cross section is only slightly curved. When the length is decreased below L_B, the instability becomes L-dependent. For intermediate length $L > L_C$, the sheet destabilizes into fundamental or higher-order buckling modes. We identify these instabilities with the bendable regime. When higher-order buckling modes develop, the critical twist and the wavelength of the wrinkles slowly but systematically decrease as the fourth-root of tension. However, it was unanticipated that the fundamental mode can develop in the bendable regime characterized by a L-dependent threshold. At even smaller length $L < L_C$ in the clamped regime, the clamped boundary conditions delays the development of the instability with greater twist required to wrinkle the sheet because the sheet is under tension near the boundaries along the transverse direction.

Thus, our experiments provide a thorough test of the scaling approach and the regimes of their applicability, as opposed to direct numerical simulations of the thin plate equations which, while accurate, give rise to less insight on the development of the instabilities, and the various operative mechanisms. This approach also yields simple forms for the dependence on material parameters. Our study provides the prefactors in addition to testing the derived scaling laws against materials with Young's modulus distributed over three orders of magnitude.

Finally, in closing, we note that the twisted ribbon configuration is an ideal experimental benchmark to test nonlinear plate models. Such work may further lead to a deeper understanding and modelling of more complex materials including fabrics [41,42], cellular solids [43], besides mechanical metamaterials [44].

Data accessibility. This article has no additional data.

Authors' contributions. A.K. and J.C. designed research; A.K. conducted experimental research; A.K. and J.C. analyzed data; A.K. and J.C. wrote the paper.

Competing interests. We declare we have no competing interests.

Funding. This work was supported by the National Science Foundation under grant number DMR 1508186.

Acknowledgements. We thank A. Panaitescu and M. Hannout for help with experiments, C. Trimble for preliminary work, and B. Davidovitch for stimulating discussions.

References

1. Coulomb CA. 1784 Recherches théoriques et expérimentales sur la force de torsion. *Mémoire de l'Académie des Sciences Paris* **66**, 229–272.
2. de Saint-Venant A. 1855 *De la torsion des prismes*. Paris, France: Imprimerie Impériale.
3. Love AEH. 2013 *A treatise on the mathematical theory of elasticity*. Cambridge, UK: Cambridge University Press.
4. Timoshenko S. 1953 *History of strength of materials: with a brief account of the history of theory of elasticity and theory of structures*. New York, NY: Dover Publications.
5. Antman SS, Kenney CS. 1981 Large buckled states of nonlinearly elastic rods under torsion, thrust, and gravity. *Arch. Ration. Mech. Anal.* **76**, 289–338. (doi:10.1007/BF00249969)
6. Thompson J, Champneys A. 1996 From helix to localized writhing in the torsional post-buckling of elastic rods. *Proc. R. Soc. Lond. A* **452**, 117–138. (doi:10.1098/rspa.1996.0007)
7. Goriely A, Nizette M, Tabor M. 2001 On the dynamics of elastic strips. *J. Nonlinear Sci.* **11**, 3–45. (doi:10.1007/s003320010009)
8. van der Heijden G, Thompson J. 1998 Lock-on to tape-like behaviour in the torsional buckling of anisotropic rods. *Phys. D* **112**, 201–224. (doi:10.1016/S0167-2789(97)00211-X)
9. van der Heijden G, Neukirch S, Goss V, Thompson J. 2003 Instability and self-contact phenomena in the writhing of clamped rods. *Int. J. Mech. Sci.* **45**, 161–196. (doi:10.1016/S0020-7403(02)00183-2)
10. Dias MA, Audoly B. 2015 'Wunderlich, Meet Kirchhoff': a general and unified description of elastic ribbons and thin rods. *J. Elast.* **119**, 49–66. (doi:10.1007/s10659-014-9487-0)
11. Chopin J, Romildo Filho T. 2016 Ordered crumpled states in twisted ribbons. (http://arxiv.org/abs/1603.02081)
12. Audoly B, Pomeau Y. 2010 *Elasticity and geometry*. Oxford, UK: Oxford University Press.
13. Friedl N, Rammerstorfer FG, Fischer FD. 2000 Buckling of stretched strips. *Comput. Struct.* **78**, 185–190. (doi:10.1016/S0045-7949(00)00072-9)
14. Cerda E, Mahadevan L. 2003 Geometry and physics of wrinkling. *Phys. Rev. Lett.* **90**, 074302. (doi:10.1103/PhysRevLett.90.074302)
15. Chopin J, Vella D, Boudaoud A. 2008 The liquid blister test. *Proc. R. Soc. A* **464**, 2887–2906. (doi:10.1098/rspa.2008.0095)
16. Vella D, Bico J, Boudaoud A, Roman B, Reis PM. 2009 The macroscopic delamination of thin films from elastic substrates. *Proc. Natl Acad. Sci. USA* **106**, 10 901–10 906. (doi:10.1073/pnas.0902160106)
17. Vandeparre H *et al.* 2011 Wrinkling hierarchy in constrained thin sheets from suspended graphene to curtains. *Phys. Rev. Lett.* **106**, 224301. (doi:10.1103/PhysRevLett.106.224301)
18. Brau F, Vandeparre H, Sabbah A, Poulard C, Boudaoud A, Damman P. 2011 Multiple-length-scale elastic instability mimics parametric resonance of nonlinear oscillators. *Nat. Phys.* **7**, 56–60. (doi:10.1038/nphys1806)
19. Davidovitch B, Schroll RD, Vella D, Adda-Bedia M, Cerda EA. 2011 Prototypical model for tensional wrinkling in thin sheets. *Proc. Natl Acad. Sci. USA* **108**, 18 227–18 232. (doi:10.1073/pnas.1108553108)
20. Taylor M, Bertoldi K, Steigmann DJ. 2014 Spatial resolution of wrinkle patterns in thin elastic sheets at finite strain. *J. Mech. Phys. Solids* **62**, 163–180. (doi:10.1016/j.jmps.2013.09.024)
21. Taylor M, Davidovitch B, Qiu Z, Bertoldi K. 2015 A comparative analysis of numerical approaches to the mechanics of elastic sheets. *J. Mech. Phys. Solids* **79**, 92–107. (doi:10.1016/j.jmps.2015.04.009)
22. Chopin J, Dasgupta M, Kudrolli A. 2017 Dynamic wrinkling and strengthening of an elastic filament in a viscous fluid. *Phys. Rev. Lett.* **119**, 088001. (doi:10.1103/PhysRevLett.119.088001)
23. Mockensturm EM. 2001 The elastic stability of twisted plates. *J. Appl. Mech.* **68**, 561–567. (doi:10.1115/1.1357517)
24. Chopin J, Kudrolli A. 2013 Helicoids, wrinkles, and loops in twisted ribbons. *Phys. Rev. Lett.* **111**, 174302. (doi:10.1103/PhysRevLett.111.174302)
25. Chopin J, Demery V, Davidovitch B. 2015 Roadmap to the morphological instabilities of a stretched twisted ribbon. *J. Elast.* **119**, 137–189. (doi:10.1007/s10659-014-9498-x)
26. Chopin J, Kudrolli A. 2016 Disclinations, e-cones, and their interactions in extensible sheets. *Soft Matter* **12**, 4457–4462. (doi:10.1039/C6SM00187D)
27. Dinh HP, Démery V, Davidovitch B, Brau F, Damman P. 2016 From cylindrical to stretching ridges and wrinkles in twisted ribbons. *Phys. Rev. Lett.* **117**, 104301. (doi:10.1103/PhysRevLett.117.104301)

28. Maurin F. 2017 Solitary waves in longitudinally wrinkled and creased helicoids. *Int. J. Non Linear Mech.* **89**, 133–141. (doi:10.1016/j.ijnonlinmec.2016.12.010)
29. Kohn RV, O'Brien E. In press. The wrinkling of a twisted ribbon. *J. Nonlinear Sci.* (doi:10.1007/s00332-018-9447-0)
30. Green AE. 1937 The elastic stability of a thin twisted strip—II. *Proc. R. Soc. A* **161**, 197–220. (doi:10.1098/rspa.1937.0141)
31. Coman CD, Bassom AP. 2008 An asymptotic description of the elastic instability of twisted thin elastic plates. *Acta Mech.* **200**, 59–68. (doi:10.1007/s00707-007-0572-3)
32. Korte AP, Starostin EL, van der Heijden GHM. 2011 Triangular buckling patterns of twisted inextensible strips. *Proc. R. Soc. A* **467**, 285–303. (doi:10.1098/rspa.2010.0200)
33. Kit OO, Tallinen T, Mahadevan L, Timonen J, Koskinen P. 2012 Twisting graphene nanoribbons into carbon nanotubes. *Phys. Rev. B* **85**, 085428. (doi:10.1103/PhysRevB.85.085428)
34. Koiter WT. 1966 On the nonlinear theory of thin elastic shells. *Koninklijke Nederlandse Akademie van Wetenschappen, Proceedings, Series B* **69**, 1–54.
35. Ciarlet PG. 2000 *Mathematical elasticity, Vol III. Theory of shells*. Amsterdam, The Netherlands: North-Holland.
36. Friesecke G, James RD, Müller S. 2006 A hierarchy of plate models derived from nonlinear elasticity by gamma-convergence. *Arch. Ration. Mech. Anal.* **180**, 183–236. (doi:10.1007/s00205-005-0400-7)
37. Blair DL, Kudrolli A. 2005 Geometry of crumpled paper. *Phys. Rev. Lett.* **94**, 166107. (doi:10.1103/PhysRevLett.94.166107)
38. Healey TJ, Li Q, Cheng RB. 2013 Wrinkling behavior of highly stretched rectangular elastic films via parametric global bifurcation. *J. Nonlinear Sci.* **23**, 777–805. (doi:10.1007/s00332-013-9168-3)
39. Nayyar V, Ravi-Chandar K, Huang R. 2011a Stretch-induced stress patterns and wrinkles in hyperelastic thin sheets. *Int. J. Solids Struct.* **48**, 3471–3483. (doi:10.1016/j.ijsolstr.2011.09.004)
40. Nayyar V, Ravi-Chandar K, Huang R. 2011b Stretch-induced stress patterns and wrinkles in hyperelastic thin sheets. *Int. J. Solids Struct.* **48**, 3471–3483. (doi:10.1016/j.ijsolstr.2011.09.004)
41. Steigmann DJ, Dell'Isola DJ. 2015 Mechanical response of fabric sheets to three-dimensional bending, twisting, and stretching. *Acta Mech. Sinica* **31**, 373–382. (doi:10.1007/s10409-015-0413-x)
42. Scerrato D, Giorgio I, Rizzi NL. 2016 Three-dimensional instabilities of pantographic sheets with parabolic lattices: numerical investigations. *Z. Angew. Math. Phys.* **67**, 53. (doi:10.1007/s00033-016-0650-2)
43. Oftadeh R, Haghpanah B, Vella D, Boudaoud A, Vaziri A. 2014 Optimal fractal-like hierarchical honeycombs. *Phys. Rev. Lett.* **113**, 104301. (doi:10.1103/PhysRevLett.113.104301)
44. Bertoldi K, Reis PM, Willshaw S, Mullin T. 2010 Negative Poisson's ratio behavior induced by an elastic instability. *Adv. Mater.* **22**, 361–366. (doi:10.1002/adma.200901956)